Jalila Kaouthar Kammoun[1], Naourez Ben Hadj[1], Moez Ghariani[1]

J. Electrical Systems 11-4 (2015): 447-462

Regular paper

Journal of Electrical Systems

Induction Motor Finite Element Analysis for EV Application, Torque Ripple and Inter-turn circuit

The use of the Induction Motor in the Electric Vehicle application presents several challenges. In this domain predictive maintenance has become a strategic notion. Economic importance of on line diagnosis of faults in electric machines gave rise to various researches in that field. This paper primarily focuses on the torque ripple reduction by varying the rotor slot geometry. Secondly it deals the Induction Motor in degraded mode in essentially the event of a short circuit between windings and between phases using finite element model of the machine. Accurate models of the Induction Machine under healthy and faulty conditions are developed using finite element method and the performance of the motor is examined. In this paper, the static two-dimensional analysis is done for stator inter turn fault and short-circuit between phases. The classical motor current signature analysis has been used to evaluate the stator current harmonic components. The machine parameters like flux linkage, flux density, are obtained for healthy and faulty motor. The results examined under various conditions are compared and the observations are presented.

Keywords: Torque ripple, Induction Motor, FEM, Electric Vehicle, Harmonic, Current density, inter-turn, short-circuit between phases

Article history: Received 16 November 2014, Received in revised form 6 November 2015, Accepted 18 November 2015

1. Introduction

Induction motors are used worldwide as the workhorse in industrial applications. Such motors are robust machines used not only for general purposes, but also in hazardous locations and severe environments essentially in Electric Vehicles (EVs) application. High Performance Electric Vehicle Systems (HPEVS) based-on 3-phase AC Induction Motor. These systems have been included into full-size vehicles, neighborhood EVs, golf carts, motorcycles, industrial/utility vehicles, high area gardening as well as in such recreational facilities as golf courses and even amusement park attractions [1]. The main reasons for adopting the IM are its ruggedness, reliability, and cost-effectiveness, which are all desired qualities for EVs and HEVs [2].

However, it is recognized that a variety of faults can occur in these motors during normal operation such as rotor fault (broken bars or end ring), stator inter-turn fault, eccentricity fault and bearing fault. A motor failure that is not identified in an initial stage may become catastrophic and the induction motor may suffer severe damage. Thus, undetected motor faults may cascade into motor failure, which in turn may cause shutdowns of VE . Such shutdowns are costly in terms of lost time, maintenance costs, and wasted raw materials.[3]

One of the most common faults in the electrical motors is the inter-turn short circuit in the one of the stator coils. The increased heat due to this short circuit may also lead to turn-turn and turn to ground faults. The inter-turn fault is mostly caused by mechanical stress, moisture and partial discharge, which is accelerated for electrical machines supplied by inverters [4].In the case of inter-turn stator winding fault, the distribution of magnetic field parameters was distorted, and the stored energy is reduced when the severity of winding

* Corresponding author: Jalila Kaouthar Kammoun email kaoutharkammoun@yahoo.fr,
[1] Electrical Engineering Department, Sfax Engineering National School 3038 Sfax, Tunisia

increases. Magneto-static analysis based on finite element analysis is used to determine the variation of the flux and stored energy in the electric machines [6]. Based on this type of analysis, the variation of the magnetic flux, magnetic flux density and stored energy can be computed accurately.

Thus, for security four-wheel, direct-drive EVs must present low torque ripple in order to reduce vibration and to provide high driving comfort. Still, some rotor shapes ushered in dangerous trouble and/or loss in torque. Therefore unsuitable rotor slot design will lead to bad torque performance and undesired noise of the IM. There are several study of improving the starting performance of the motor as well as the efficiency and torque outcome by varying rotor slot type & shape (See [2], [6], [7], [8] and [9]).

In this paper, the impact of rotor geometry parameters like rotor slot type & shape, number of rotor slot on the efficiency, torque performance and electromagnetic noise is discussed. The advantages and disadvantages of them are indicated. Comparing torque and harmonic specific to a rotor's current density of different rotor slot shapes, the optimal value is achieved by Finite Element Analysis [5]. The latter is a established numerical tool for the analysis of electromagnetic phenomena in electrical machines and devices and a valuable tool for motor design. Two analyses are carried out: the no-load test conducted first, then the locked rotor [13]. Consequently, the control of the current density harmonic in slot rotor is necessary in the case of both a healthy and an unhealthy IM. Simulation results prove that the optimal form of rotor slots is the round shape since the gain in torque ripple peak to peak may reach 40% compared to the rectangular shape. Besides, the Total Harmonic Distortion (THD) is significantly attenuated.

Furthermore, in the current paper, FEM has been used to simulate and detect the main types of faults in three-phase induction machines. FEM is used to build the complex geometry of the model, and the type of materials is selected to specify the stator windings, rotor windings and iron cores. As a result, all electrical and mechanical faults types can be modeled smoothly based on this numerical method. Motor current signature analysis (MCSA) has been used to give a decision about the fault occurrence. It has been found that the inter-turn short circuit faults have a sideband harmonic component at k = 3.

2. Notation

The notation used throughout the paper is stated below.

Indexes:

H	Magnetic field intensity
J	Magnetic field density
B	Magnetic flux density
A	Vector potential
Tslot	Torque ripple
μ	Permeability
f (Hz)	Frequency
Is (A)	Current
λa(Wb)	a-phase flux linkage (real and imaginary part)
T (N.m)	Torque computed from Maxwell stress tensor
Wm (J)	Magnetic energy
W'm(J)	Magnetic coenery
WAJ(J)	Integral of A. J

3. Definitions and pre-processing

In this paper, two analyses are carried out using finite magnetic method: at first the no-load test, then the locked-rotor test are simulated. At no-load, magneto-static simulations are carried out varying the magnetizing current.
In the locked-rotor test, the frequency is changed so as to compute the dependence of the rotor parameters on the operating frequency.
From these two tests, the parameters of the equivalent circuit of the induction motor are obtained, from which the motor performance can be predicted. Among the others, the energy, co-energy and the torque produced.

3.1. Definition of IM materials

The structure of the induction motor under analysis is shown in Fig. 1 which also highlights the materials of the various blocks. Particular care has to be given to the materials used in the simulations. In particular
Copper: The stator and the rotor slot are filled by several wires. However, it is considered that the slot is completely filled by copper, considering an equivalent conductive bar. In this bar the total current of all the wires is assigned. In the magneto-dynamic computation, this yields a non-uniform distribution of the stator current within the slot, according to the operating frequency. In order to avoid this mistake, the conductivity of the copper can be equated to zero, yielding an infinite penetration thickness.
Steel 1010: The steel non-linear characteristic (the B-H curve) has to be used in the no-load simulation. However the higher values of the curve are not always available and they are interpolated during the finite element analysis. It is convenient to assign the high values of flux density B and magnetic field H when they are not given, extending the curve with a slop close to the $\mu 0$. An example of B-H curve is given in Table 1.
At last, in the magnet-dynamic simulations of the locked-rotor tests a linear characteristic for the Steel 1010 can be adopted, so as to limit the research to the effect of the frequency on the rotor parameters.

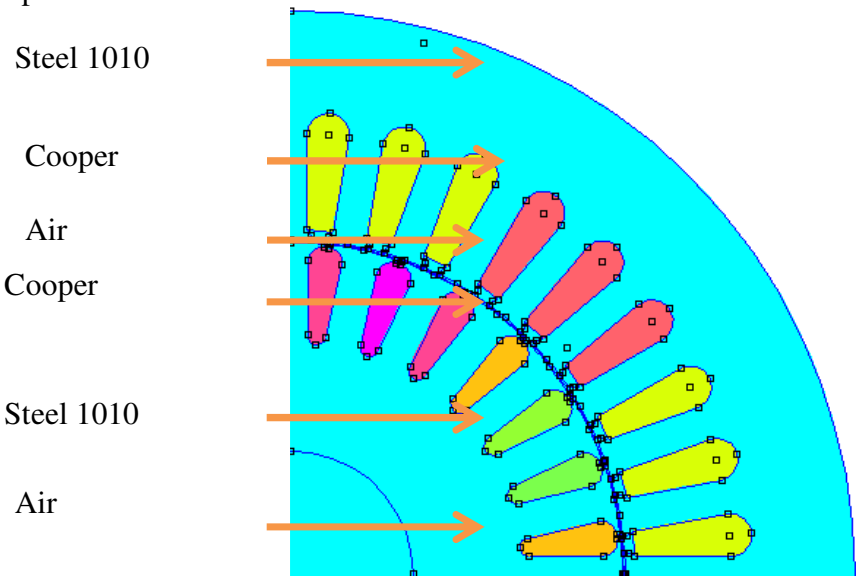

Fig 1.Materials in the simulation

Table 1: Example of B-H curve of Steel 1010

B (T)	*H*(A/m)	*B* (T)	*H*(A/m)	*B* (T)	*H*(A/m)
0	0	0.931	795.80	1.698	6366.20
0.2003	238.700	1.1014	1114.100	1.730	7957.70
0.3204	318.300	1.2016	1273.200	1.870	15915.50
0.400450	358.100	1.3020	1591.500	1.990	31831.00
0.500550	437.700	1.4028	2228.200	2.040	47746.50
0.56060	477.500	1.524	3183.100	2.070	63662.00
0.79080	636.600	1.626	4774.600	2.095	79577.50

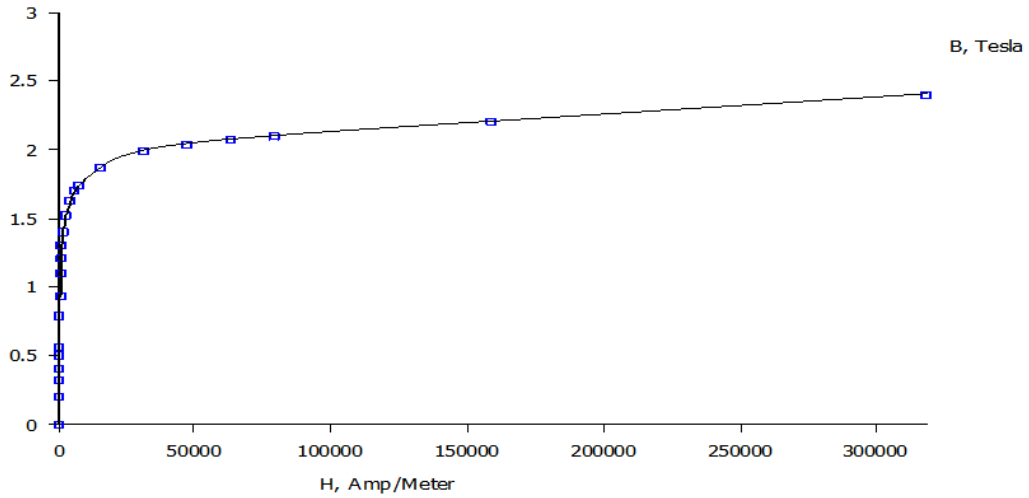

Fig.2.B-H curve of Steel 1010

3.2. No-Load Test

The simulations are realized at zero frequency, assuming to work in the rotor reference frame. This corresponds to a rotor slip *s* equal to zero. Thus a magneto-static field problem is solved. Stator currents are imposed and the non-linear comportment of the magnetizing inductance is calculated. A series of simulations are carried out varying the stator current. The non-linear characteristic of the steel has to be used in the simulation. Fig.3 illustrates the flux plot during the no-load test.

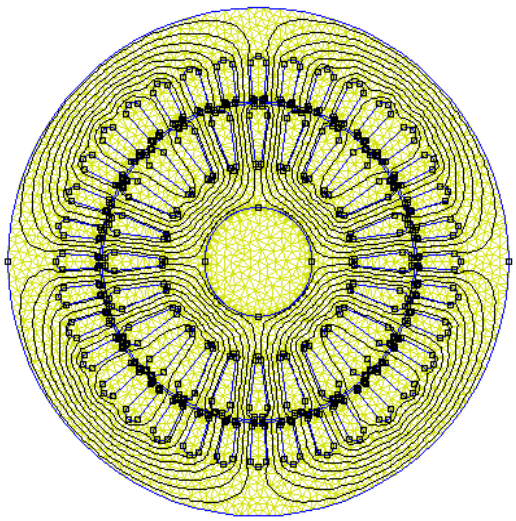

Fig.3. Map of Flux density under no-load test

Fig. 2 shows the magnetic energy versus the stator current. It is worth noticing that different computation yield different results in the saturation region. The computation of the whole magnetic energy cannot be used. Its value becomes lower and lower with the saturation and cannot more used for the computation of the magnetizing inductance. [18]

$$W_{AJ} = \int_{vol} \int_{0}^{B} HdB\,dvol \tag{1}$$

On the contrary, the apparent energy can be used to estimate the apparent magnetizing inductance of the machine.

$$W_{AJ} = \int_{vol} AJdvol \tag{2}$$

It can be also observed that

$$W_{AJ} = W_m + W'_m \tag{3}$$

Where W'_m is the magnetic co-energy

$$W'_m = \int_{vol} \int_{0}^{B} BdH\,dvol \tag{4}$$

A numerical comparison is given in Table 1. At low currents it is observed that $W_m = W'_m = 0.5 * W_{AJ}$ while this is not hold at higher currents.

As validation of this remark, Fig 4 indicates the magnetizing inductance computed using two different ways. Using the flux-linkage or the energy yield a correct value of its apparent inductance:

$$L_m = \frac{2}{3}\frac{W_{AJ}}{I_0^2} \tag{5}$$

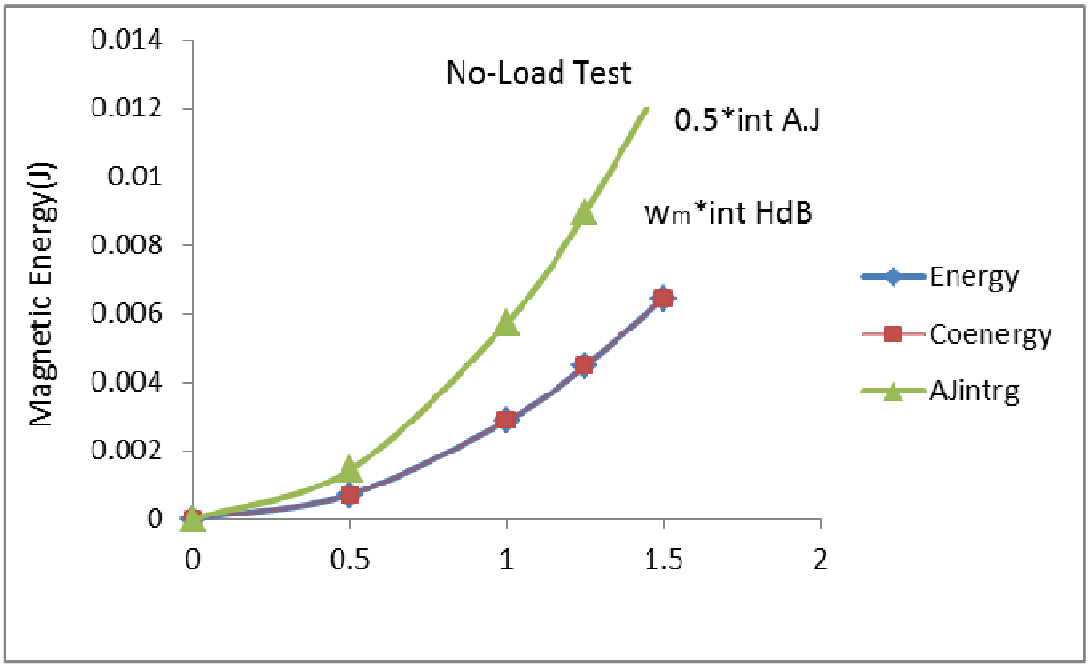

Fig.4. Energy and co-energy versus stator current

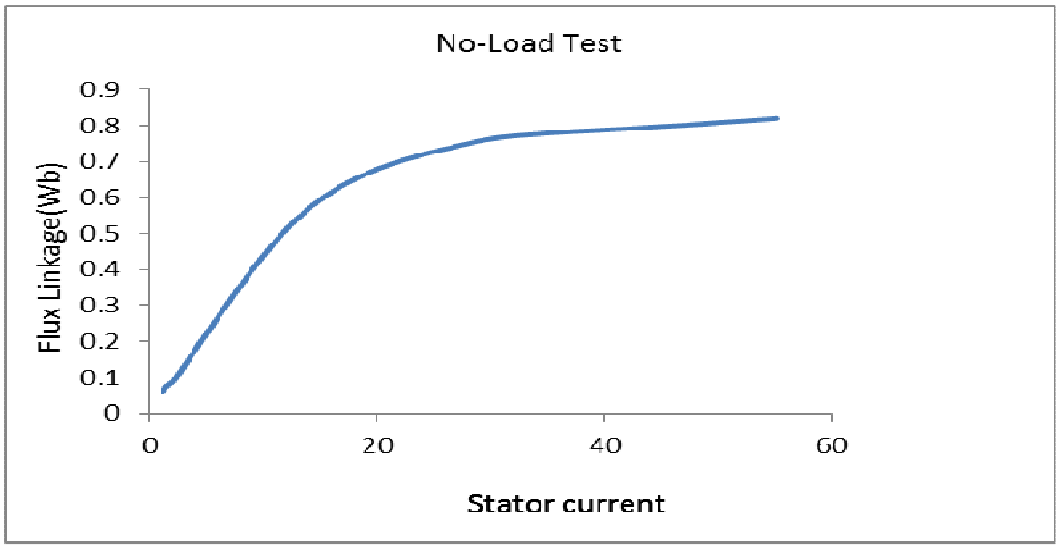

Fig.5. Flux linkage versus stator current

Referring to the *a* phase, the magnetizing inductance is computed as

$$L_m = \frac{\lambda a}{Ia} \tag{6}$$

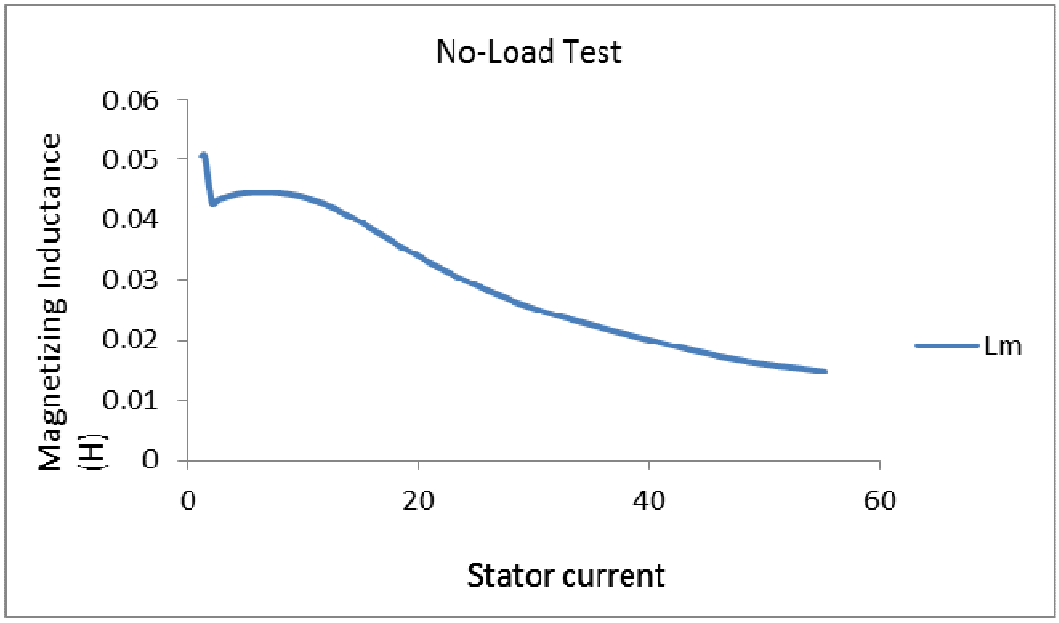

Fig.6. Magnetizing inductance versus stator current

Table II Magnetic Energy Comparison

Isim (rms) (A)	Energy W_m (J)	Co-energy W'_m (J)	AJintrg W_{AJ} (J)
0	0	0	0
0.5	0.00071642	0.00071642	0.00143283
1	0.00286572	0.00286568	0.0057314
1.25	0.00447775	0.00447764	0.00895539
1.5	0.00644805	0.00644784	0.01289589
2	0.01146366	0.01146297	0.02292663

3.3. Locked rotor test

These tests are carried out supposing a locked-rotor and imposing a fixed current within the stator slots. A series of simulations are recognized at several frequencies so as to weigh up the dependence of the rotor parameters on the operating frequency.
In these simulations the steel 1010 is assumed to be linear, so as to allow the superposition of the effect to be applied. The corresponding magnetizing inductance is fixed to its linear value. This assumption does not affect the computation since the main purpose of this test is to compute the rotor parameters.
As an example, Fig. 7 and Fig. 8 show the flux plots during the locked-rotor test at two different frequencies: at 0 Hz and at 25 Hz, respectively. It is worth noticing the higher shielding effect of the rotor current at the higher frequency.

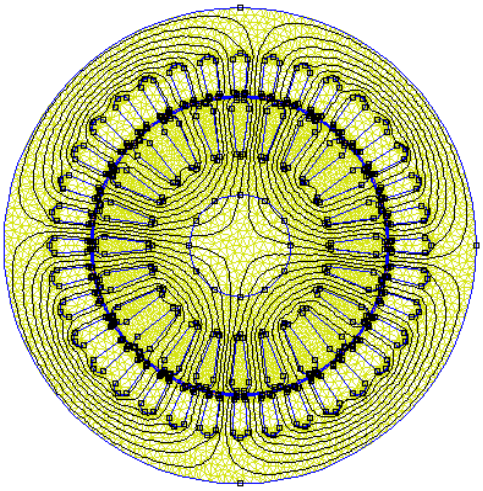

Fig7.Map of flux density under locked rotor test (0 Hz)

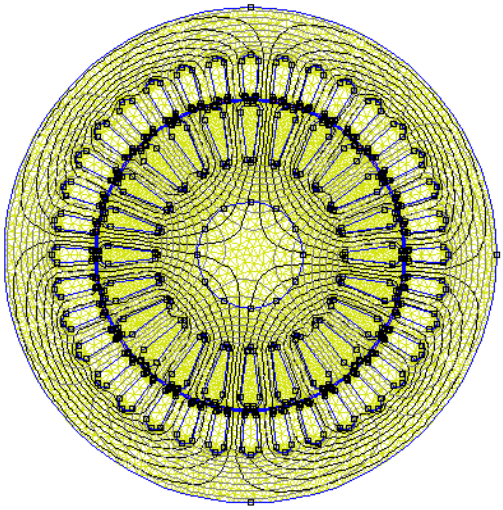

Fig8.Map of flux density under locked rotor test (25 Hz)

Fig. 9 shows the magnetic energy computed in different ways. In this case, the motor works in linear conditions, so that the computation yields the same result.
Fig. 10 shows the computed torque as a function of the working frequency. It is worth noticing that the torque computed here refers to a constant current source, fixed in all the simulation, and then it has not to be confused with the torque obtained at fixed voltage to plot the mechanical characteristic of the machine.
The Maxwell stress tensor is computed along a line within the air-gap of the motor. The torque is also proportional to the power transferred from the stator to the rotor.

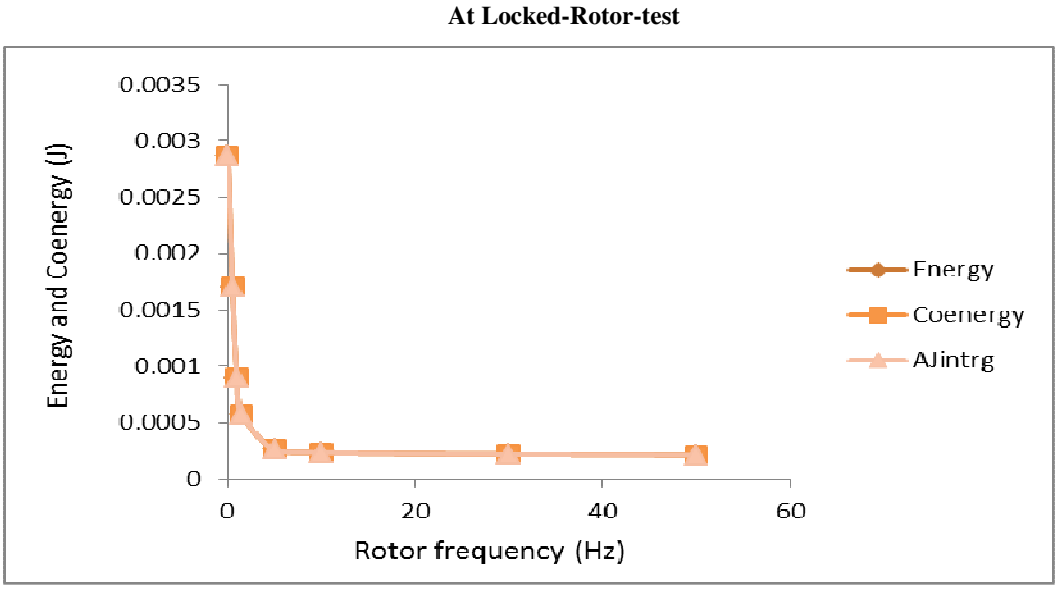

Fig.9. Energy versus frequency

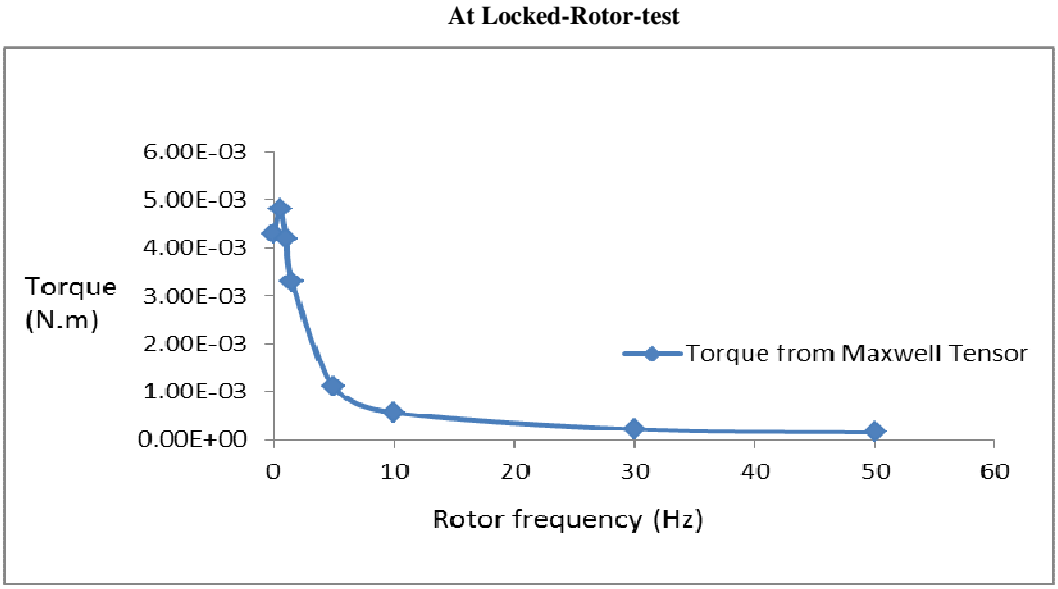

Fig.10. Torque versus frequency

3. Torque Ripple

Control need and operational environments of electric machines for EV drives are dissimilar from that of the traditional electric machines. Ideal torque-speed characteristic of the EV traction motor is constant -torque operation below base speed and constant-power operation above base speed. Low vibration /noise and high efficiency are likewise important for the EV drives. Throughout the IM design, it is found that the type, shape and number of rotor slots have great impact on these characteristics. Thus, these parameters must be designed properly. If this condition is not satisfied the IM will have torque decline phenomenon during high speed operation and big vibration/noise. Moreover, it is important to optimize these parameters. It is analyzed that the influences of rotor slot type, rotor slot shape, torque performance and electromagnetic noise. As explained by *Kamoun et al.* [13],[14] the ripple torque (T-slot) is the main result of the magnetic variation energy stored

in the air gap. It is mainly caused by the movement of the rotor slots and the stationary stator slots. It appears that, due to the interaction between the rotor magnetic flux and slotting, the stator reluctance varies.

By using the Fourier transformation of the electromagnetic field, the induction motor is analyzed by the nonlinear time-stepping, finite-element analysis to obtain the results of the harmonic fields with enough accuracy [20].
Rotor slot type effects the distribution of the magnetic field to a degree. Even a little difference of the magnetic field distribution introduces big difference on the performance of the IM. Fig.11and12 are IM field distribution of both rotor slot types.

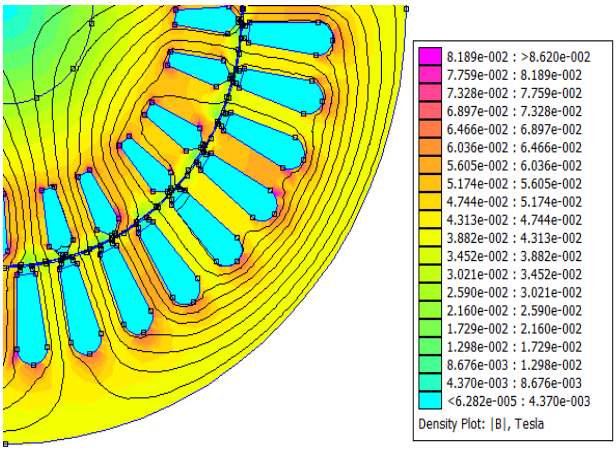

Fig.11. Flux distribution at IM with rectangular rotor slot

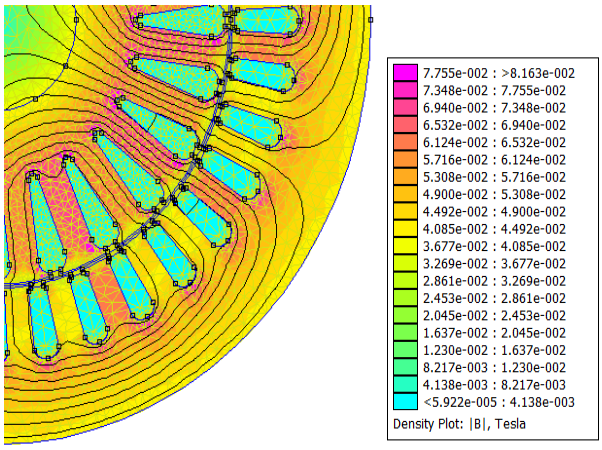

Fig.12. Flux distribution at IM with round rotor slot

The torque ripple can be predicted either analytically [19–21] or by using numerical tools such as finite element simulations [21–24]. For the purposes of the current project, a 2-D FEA study with FEMM 4.2 soft of the four IM configurations is conducted. This numerical method solves the Maxwell equations for each mesh surface element. The different simulations performed together with the achieved results are reported on in the following section.

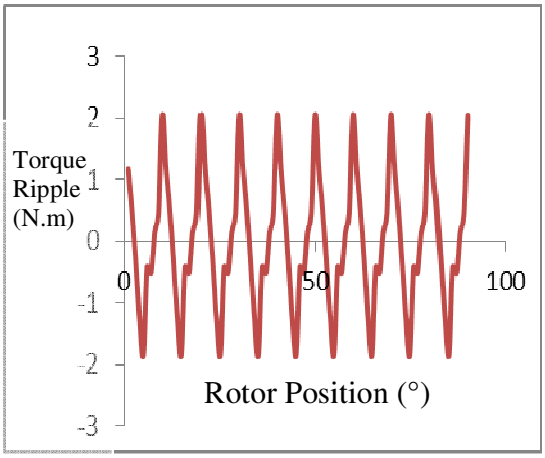

Fig.13. Torque Ripple of the IM with Rectangular Rotor Slots

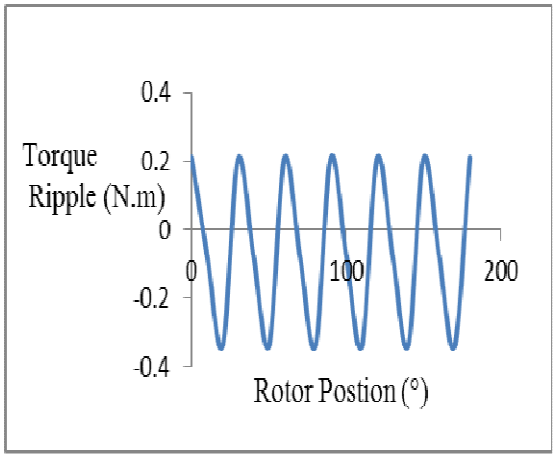

Fig.14. Torque Ripple of the IM with Round Rotor Slots

The ripple torque of IM peak to peak can be expressed by the following equation [19]:

$$T_{slot-pp} = Max\,(T_{slot}) - Min\,(T_{slot})$$

Considering Equation 12 and Figure 13, the torque slot is periodic with a period equal to 10°. Then, we can limit our study to a rotation of 10°, which reduces the time of FE analysis.

The maximum recorded peak-to-peak ripple torque is equal to 0.4 N.m, as can be noticed in Figure 13, but, for the rectangular Rotor Slots, the maximum recorded peak-to-peak torque ripple is more than 3N.m as it is shown in Figure 10. The nominal torque of the prototype machine is 29.8 N.m. All these results warrant the conclusion that the design of the rotor slots significantly affects the shape of the ripple torque curve.

Since the IM with round rotor slot delivers a ripple torque lower than the structure with rectangular rotor slot as is proven in earlier work Kamoun [14] we chose this structure for detecting IM faults.

4. FEM IM inter-turn fault model and field study

Inter-turn short circuits in stator windings constitute a category of faults that is most common in IMs. Majority of motor stator winding failure occurs due to the destruction of the turn insulation produced by the short circuit in stator windings. The type of shorts could be of the following types [22]:

i. Inter-turn shorts of same phase
ii. Short between coils of same phase
iii. Short between two phases
iv. Short between phase to earth.

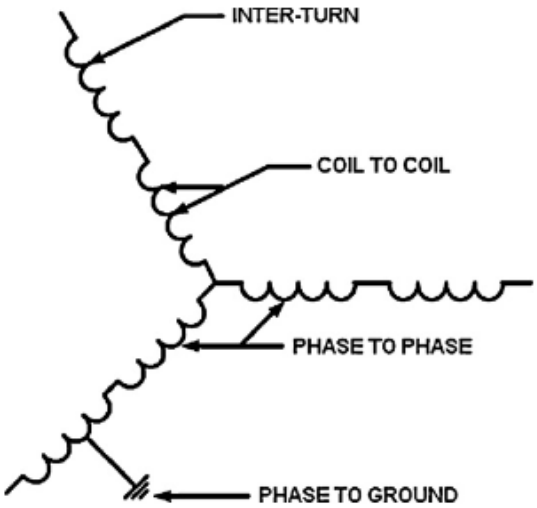

Fig. 15. Schematic diagram of different stator short possibilities.

.

Figure 15 shows the schematic diagram of the different types of stator winding problems except open-circuit of the stator coil. Several studies [24] report that depending on the type of shorts, and condition of motor (age, working condition, etc.), the motor may continue to operate initially, even though short-circuit current will flow, causing more and more overheating, ultimately leading to complete failure if not accounted for. The studies [25, 26] also point that with the inter-turn and coil short of same phase, the motor might still continue to run. The detrimental ones are the short between the phases and phase-to-earth, causing instantaneous motor shut down. About the failure mode trend, it is generally argued that the shorts in a particular phase, if undetected, would grow onto phase-to-phase faults.

Although there are no exclusive data to indicate the transition time between inter-turn (in same phase) and ground wall (between phase-to-phase) insulation failure [25], however, detection of inter-turn shorts during motor operation would reduce the damage to adjacent coils and the stator core, reducing repair cost and motor outage time.

We are interested in this paper to detect a short circuit between turns which denotes an insulation failure between two windings in the same phase of the stator. The insulation failure is modeled by a resistance, where its value depends on the fault severity. The stator winding of an IM machine with inter-turn fault is represented in Fig. 16.

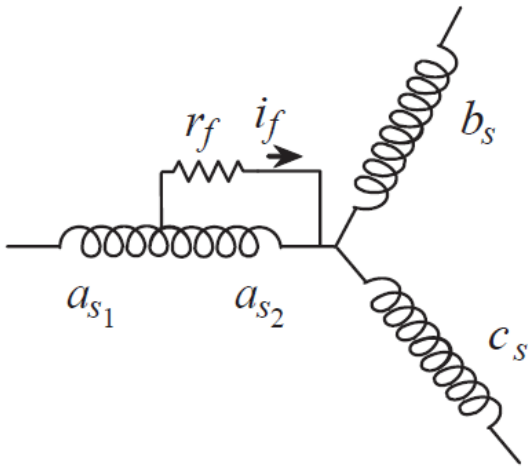

Fig.16. Stator circuit of IM with inter-turn fault in the phase as.

In this figure, the fault is happened in the phase as and rf characterizes the fault insulation resistance. The sub-windings (as1) and (as2) represent the healthy and faulty part of the phase winding a respectively. When fault resistance (rf) decreases toward zero, the insulation fault evaluates toward an inter-turn full short-circuit. The evolution between rf = 1 and rf = 0 is very fast in most insulation materials.

In order to simulate and analyze the performance of electric machine a 2-D FEM was used. Solution of electromagnetic filed equations provides acceptable information about healthy and inter-turn short circuit. The winding in each phase was divided into different groups in order to model the different types of short circuit fault. The coils of stator phases are divided into two parts connected in series with equal turns for each part. By this method, a short circuit can be implemented at any location of the coil [27].

4.1. Simulation of IM with stator inter-turn fault

Inter-turn fault occurs due to the failure of insulation in the windings. The studied IM has 36 slots and 4 poles. The winding diagram of the studied IM is illustrated in Fig.17.

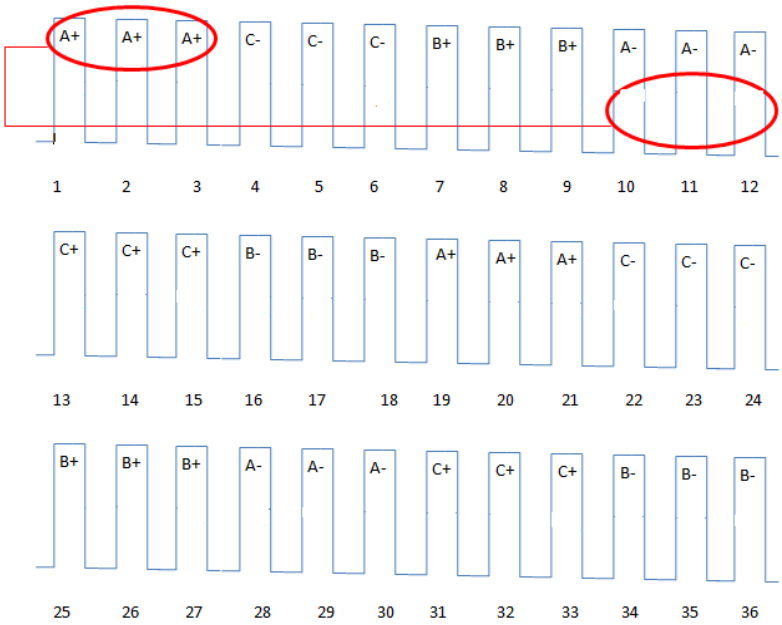

Fig.17. Winding diagram of the studied IM

In order to execute the inter-turn fault, the winding where the fault occurs, is shared into two portions which are associated to 2 sub-windings connected in series (as1, as2). With such a procedure, the magnetic flux linked with each winding branch is accessible. In the coupled electrical circuit the fault part of phase winding is short-circuited with a fault insulation resistance.

The portion of faulty turns in stator winding inter-turn fault is considered 16.67% of phase as winding. The magnetic flux distribution of healthy and faulty IM is shown in Fig. 18. It is seen that the flux distribution is symmetrical in the case of healthy machine while it becomes asymmetrical for the machine with inter-turn fault.

It is seen that the path and polarity of flux is changed near faulty slot windings. Comparing the magnetic flux distribution of healthy and faulty machines helps to detect the influence of turn fault. The deviation of flux distribution leads to vibration torque; noise and un-unified magnetic stress depend on the fault severity.

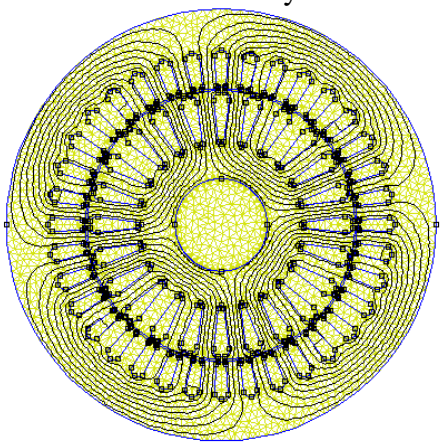

Fig. 18. Magnetic Field and Flux Distribution under Healthy Conditions

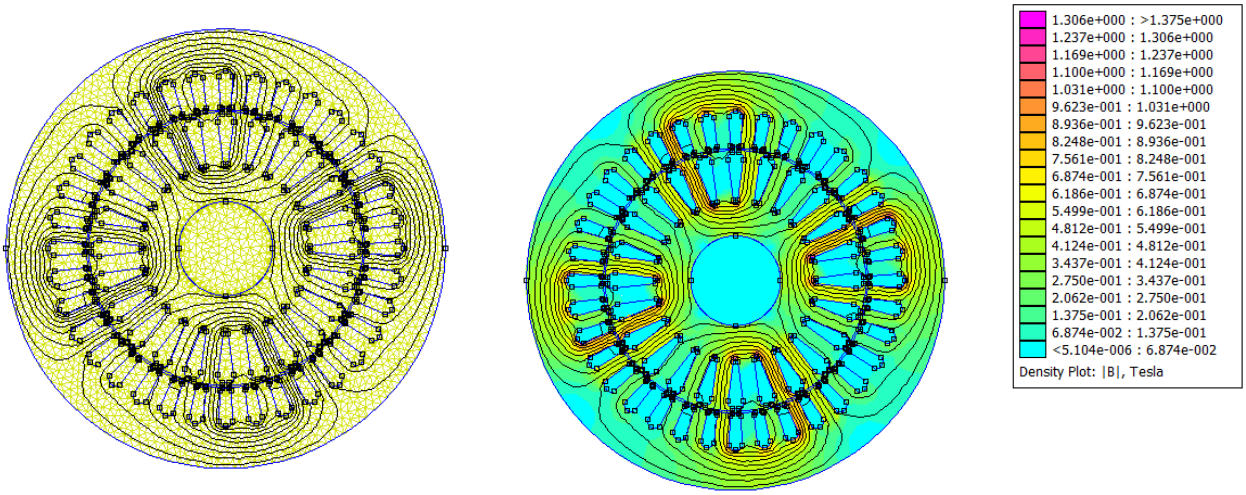

Fig. 19. Magnetic Field and Flux Distribution under inter-turn Fault Conditions

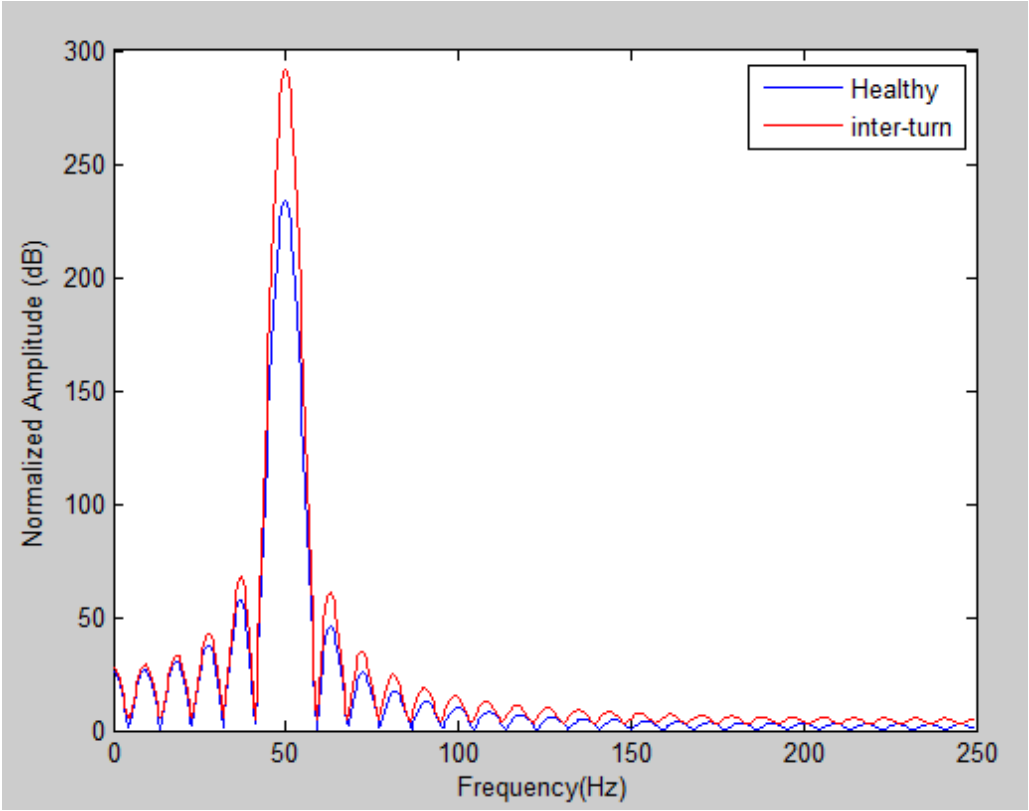

Fig.20. Stator Current Spectra under inter-turn circuit

Figure 20 shows the harmonic spectra of the stator phase current for a fault in the operating point. It is noted that the amplitude of the different harmonics are very low and the current is almost sinusoidal. This is not entirely true for lower fault resistances for current distortion becomes more important. However, we note the existence of harmonic three defaulted presence, the harmonic does not appear when the stator currents form a balanced system (sound machine).

An inter-turn short circuits in stator windings causes a current flow in the defect turns; the amplitude of this current can be very important. Moreover it produces harmonics around the fundamental as shown in fig.20 for a frequency of 40 and 60 Hz.

The Total Harmonic Distortion (THD) block measures the total harmonic distortion of a periodic distorted signal. The signal can be a measured current.

The THD is defined as the root mean square (RMS) value of the total harmonics of the signal, divided by the RMS value of its fundamental signal. For example, for currents density, the THD is defined as

Total harmonic distortion : $$THD = \frac{J_H}{J_F}$$

$$J_H = \sqrt{J_2^2 + J_3^2 + \ldots + J_n^2)}$$

The THD of healthy signal is equal to 22.01% but the THD of stator current affected by inter-turn is equal to 52.92%.

4.2. Simulation of IM with stator short circuit between phases

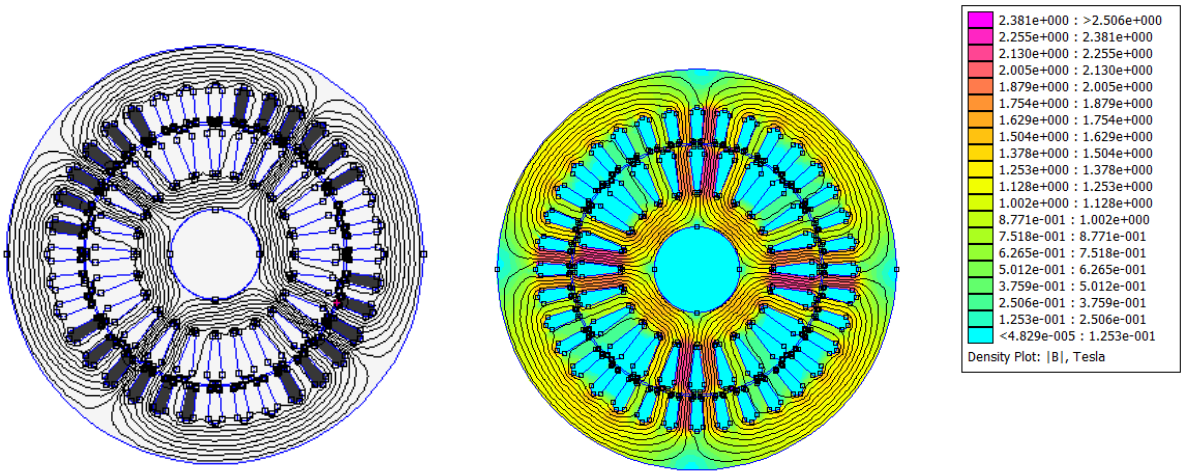

Fig.21. Magnetic Field and Flux Distribution under Short circuit between phases Fault Conditions

In the case of a short circuit between phases distribution of flux lines in the air gap becomes non-uniform as is shown in fig.21. The stored magnetic energy decreases as the percentage of fault in the stator increases. The flux density also decreases proportionally to the fault.

The short circuit between phase can reach any point of the coil, except that the effects will not be the same depending on the location. Therefore, it is laborious to analyze the impact of this type of fault on the system.

Among the effects of a short circuit near the power between phases is announced:

• Elevated currents that would lead to the fusion of the supply conductors and/or disconnection by the protections.

And among the serious results of a near neutral short circuit between two phases is reported

• A phase current imbalance with a lower risk of the fusion of conductors.

In this case THD value of waveform which present short-circuit between phases is around 61.75%.

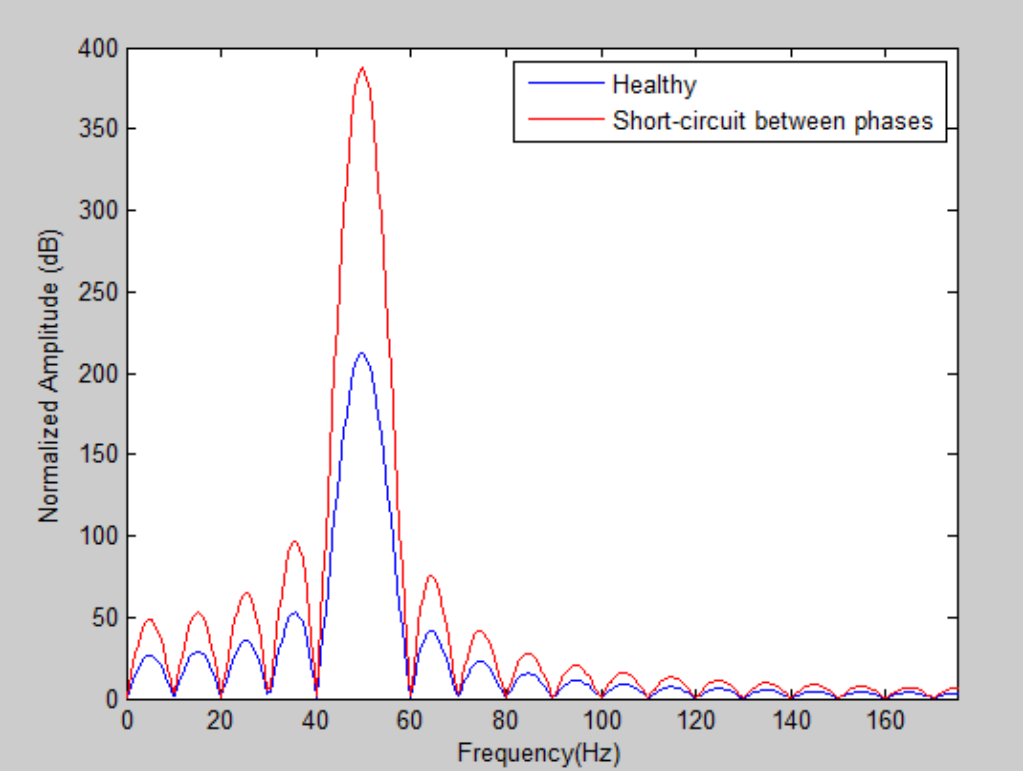

Fig.22. Stator Current Spectra under Short circuit between phases

5. Conclusion

Finite element method was used to determine firstly the magnetic field distribution both in no-load test, locked rotor test in order to define IM parameter.

Secondly, using FEM the magnetic field distribution is presented for healthy IM and the IM having two defaults; inter-turn and short-circuit between phases.

In this paper, the specifications of the two topologies of IM are presented, the influence of rotor slot shapes on flux lines and torque ripple are studied. Using FEM comparative analysis, between both torque ripple is presented. In fact, the round shape enables a gain in torque ripple peak to peak that may reach as high as 75% compared to the rectangular shape.

The presented FEM analysis is one effective and inexpensive method for studying the influence of stator faults on behavior of three phase induction machines. This method also allows studying the effect of stator faults on stator line currents, applicable on developing effective fault diagnostic tools. Once again it has been proved that the THD of waveform with inter-turn is equal to 52.92% however the THD of waveform with short-circuit between phases is superior than THD of waveform with inter-turn is equal to 61.75%.

Furthermore, based on the rules for calculating the harmonics produced in stator line currents generated in the case of inter-turn-circuit and short-circuit between two phases there are also two sidebands components in the spectrum on (40and 60) Hz.

The harmonic component depends on the degree of each fault type. In order to distinguish between the two fault types; inter-turn-circuit and short-circuit between two phases, it is necessary to compare the amplitude of the stator current in time domain.

References

[1] J. Guzinski, H. Abu-Rub, Sensorless induction motor drive for electric vehicle application, International Journal of Engineering, Science and Technology Vol. 2, No. 10, 2010, pp. 20-34
[2] M. A. Herwald, Control Design and analysis of an advanced induction motor electric vehicle drive, thesis 29 April 1999.
[3] B. Vaseghi, N. Takorabet, and F. Meibody-Tabar " Transient Finite Element Analysis of Induction Machines with Stator Winding Turn Fault" Progress In Electromagnetics Research, PIER 95, 1-18, 2009
[4] Aderiano M. da Silva, B.S."Induction motor fault diagnostic and monitoring method", thesis May 2006
[5] C. Shumei, D. Ying, S. Liwei, Rotor Slots Design of Induction Machine for Hybrid Electric Vehicle Drives, IEEE, Vehicle Power and Propulsion Conference, VPPC'06, 2006
[6] B. Virlan, A. Simion, L. Livadaru, A. Muteanu, A. M. Mihai and S. Vlasceanu, External Rotor Shape Estimation of an induction motor by FEM Analysis octombrie-decembrie, Buletinul AGIR nr. 4/2011 nr.
[7] M. Afaque Iqbal, G. Singh, Review on Influence of Rotor Geometry on the Performance of Single-Phase Capacitor-Run Induction Motor, International Journal of Advanced Research in Electrical, Electronics and Instrumentation Engineering , June 2014.
[8] V. Fireteanu, T. Tudorache and O. A. Turcanu, Optimal Design of Rotor Slot Geometry of Squirrel-Cage Type Induction Motors Romania, 1 -4244-0743-5/07/2007 IEEE.
[9] V. A. Galindo, X. M. Lopez-FDEZ, J. A. DiasPinto and P. Coimbra, Parametric study of rotor slot shape on a cage Induction Motor, 2000.
[10] J. Guzinski, H. Abu-Rub**,** Calculation of Electromagnetic Fields in Electrical Machines using Finite Elements Method, International Journal of Engineering and Industries, volume 2, Number 1, March, 2011.
[11] K. J. Hammadi, S. Hachem Farhan, M. Ibrahim Gamai, Analysis AND Monitoring Characteristic Performance OF Squirrel-Cage Induction Motor WITH Broken Bars, Journal of Engineering and Development, Vol. 17, No.3, August 2013, ISSN 1813- 7822
[12] K. Yamazaki, A. Suzuki, M. Ohto and T. Takakura, Harmonic Loss and Torque Analysis of High Speed Induction Motors, 978-1-4577-0541 IEEE, 2011.
[13] J. K. Kamoun, N. Ben Hadj, M. Chabchoub, R. Neji, and M. Ghariani, An Induction Motor FEM-Based Comparative Study: Analysis of Two Topologies, Eighth International Conference and Exhibition on Ecological Vehicles and Renewable Energies (EVER), March 2013.
[14] J. K. Kamoun, N. B. Hadj, M. Ghariani, R.Neji "Torque Ripple and Harmonic Density Current Study in Induction Motor: Two Rotor Slot Shapes", *International Review on Modelling and Simulations (I.RE.MO.S.), Vol. 8, N. 2 ISSN 1974-9821 April 2015*
[15] D. A. González, J. A. Tapia, and A. L. Bettancourt, Design Consideration to Reduce Cogging Torque in Axial Flux Permanent-Magnet Machine, IEEE Trans. Magn., vol. 43, no. 8, pp. 3435‐3440, Aug,2007.
[16] L. Dosiek and P. Pillay, "Cogging Torque Reduction in Permanent Magnet Machines," IEEE Trans. Ind. Appl., vol. 43, no. 6, pp. 1565–1571, Nov./Dec.2007.
[17] S. Williamson, C. I. McClay, "Optimisation of the geometry of closed rotor slots for cage Induction Motors, Industry Applications Conference Thirtieth IAS Annual Meeting, IAS'95., IEEE, Volume: 1,1995.
[18]N. Bianchi L. Alberti "Finite element analysis of the induction motor", June 1, 2006
[19] H. Jia, M. Cheng, W. Hua, W. Zhao, and W. Li, "Torque Ripple Suppression in Flux-Switching PM Motor by Harmonic Current Injection Based on Voltage Space-Vector Modulation," IEEE Trans. Magn., vol. 46, no. 6, pp. 1527‐1530, Jun. 2010.
[20] L. Zhu, S. Z. Jiang, Z. Q. Zhu and C. C. Chan, "Analytical Methods for Minimizing Cogging Torque in Permanent-Magnet Machines," IEEE Trans. Magn., vol. 45, no. 4, pp. 2023‐2031, Apr. 2009.
[21] K. Lu, P. O. Rasmussen and E. Ritchie, An Analytical Equation for Cogging Torque Calculation in Permanent Magnet Motors," 17th International Conference on Electrical Machines, Chania, Kreta,Grækenland, 2006.
[22] A. Kiyoumarsi, Prediction of Torque Pulsations in Brushless Permanents-Magnet Motors Using Improved Analytical Technique, Journal of Electrical Engineering, vol. 61, no. 1,pp. 37‐43,2010.
[23] S. Rashidae and S. A. Gholamian,"Reduction of cogging Torque in IPM Motors by Using the Taguchiand Finite Eement Method," International Journal of Computer Science & Engineering Survey, vol. 2, no.2, May 2011
[25] C. Y. Hsiao, S. N. Yeh and J. C. Hwang, A Rapid Simulation Method for Cogging Torque Calculation of Permanent-Magnet Synchronous Machines, The 32nd symposium on electrical power engineering, Taiwan's new North City, 2-3 December 2011.
[26] A. Kumar, S. Marwaha and A. Marwaha, "Comparison of methods of minimization of cogging torque in wind generators using FE analysis," Journal Indian Institute of Science, vol. 86, pp. 355-362 Jul./Aug. 2006.
[27] K. Yamazaki, Y. Haruishi, and T. Ara, Calculation of Negative Torque Caused by Slot Ripples of Induction Motors, IEEE Transactions on magnetics, VOL. 40, NO. 2, MARCH 2004.